Journal of Catalysis **194,** 309–317 (2000)
doi:10.1006/jcat.2000.2937, available online at http://www.idealibrary.com on IDEAL®

Characterization and Kinetic Studies on the Highly Active Ammoxidation Catalyst $MoVNbTeO_x$

Kiyotaka Asakura,*[,1] Kaori Nakatani,† Takeshi Kubota,†[,2] and Yasuhiro Iwasawa†[,3]

*Research Center for Spectrochemistry and †Department of Chemistry, Graduate School of Science, The University of Tokyo, Hongo, Bunkyo-ku, Tokyo 113-0033, Japan

Received February 7, 2000; revised May 24, 2000; accepted May 24, 2000

The catalytic performance and structures of multicomponent "MoVNbTe" oxides have been studied to find the correlation among the performance, active phases, and preparation conditions. The catalyst with the composition $MoV_{0.4}Nb_{0.1}Te_{0.2}O_x$ showed high activity and selectivity for propane ammoxidation reaction (ca. 50% selectivity to acrylonitrile at ca. 90% conversion) when it was pretreated at 830–900 K for 2 h under O_2-free or less than 100 ppm O_2-contaminated N_2 or He flow conditions. Active phases were characterized by XRD, which gave $2\theta = 14.1^\circ$, 24.9°, 26.9°, 29.1°, 32.4°, 33.2°, and 35.4° in addition to the peaks at 22.1°, 28.2°, 36.2°, 44.7°, and 50.0° reported previously. XPS revealed the presence of Mo^{5+} in addition to Mo^{6+}. In the presence of more than 1000 ppm O_2 contamination during the pretreatment, α-MoO_3 was formed at the surface region, resulting in reduction of the activity for propane ammoxidation. The activation energy for propane conversion was 32.0 kcal/mol, which was a little smaller than the 36.1 kcal/mol for propene ammoxidation. The reaction rate (v) for propane ammoxidation on the MoVNbTe oxide catalyst at 693 K is given by $v = k\,[\text{propane}]^{0.8}\,[O_2]^{0.4}\,[NH_3]^{-0.4}$. The active phases and reaction mechanism are discussed on the basis of the characterization by XRD and XPS and the kinetic data. © 2000 Academic Press

Key Words: **ammoxidation; acrylonitrile; propane; XPS; XRD; kinetics; MoVNbTe oxide catalyst.**

INTRODUCTION

Acrylonitrile is an industrially important basic chemical for the production of polymers and rubbers, and it is efficiently produced by propene ammoxidation using multiphase-multicomponent catalysts (1–3). Due to increasing economic demand, however, catalysts which produce acrylonitrile directly from propane have been studied extensively (1, 3, 4). The achievement of propane ammoxidation requires severe reaction conditions because of the lower reactivity of propane compared to propene, e.g., the higher temperatures at which the complete oxidation to CO_2 may proceed. Recently, several reviews have been presented on effective catalysts for the selective oxidation of propane to acrylonitrile (1, 3–9). Kim *et al.* reported that AgBiVMoOx gave 64.9% of acrylonitrile selectivity at 15.8% propane conversion (10). In this catalytic system, however, propane is dehydrogenated to propene in the gas phase and the propene is ammoxidized to acrylonitrile on the catalyst. A $VSbWP/Al_2O_3$ catalyst among the VSb-based oxides reported showed 85% conversion with 37% acrylonitrile selectivity (11–13). V is active for propane oxidative dehydrogenation, while Sb is active for propene ammoxidation (14, 15). We found Pt/SbO_x catalysts which were active for the synthesis of acrylonitrile from propane or methacrolein from isobutane, where Sb suboxide species cover a part of the Pt particle surface to suppress the undesired C–C bond breaking and complete combustion of the hydrocarbons (16–19). Irrespective of many efforts toward the development of selective ammoxidation catalysts, improvement of the performance is still an important challenge that is of interest from both fundamental research and industrial points of view. Recently, Ushikubo and coworkers discovered a new catalytic system of MoVNbTe oxides (20–22). This catalyst shows a high selectivity toward acrylonitrile (>50%) at a propane conversion of more than 90%. It can be operated at relatively lower temperatures (683–723 K) compared to the other propane ammoxidation catalysts (23). However, there are few available studies about this catalyst, and the origin of such excellent catalysis remains still unknown (24, 25).

In this paper we report on the kinetic study of propane ammoxidation on the MoVNbTe oxide catalyst and the correlation between the surface composition and structure and the catalytic performance.

EXPERIMENTAL

An $MoV_{0.4}Nb_{0.1}Te_{0.2}O_x$ catalyst was prepared in a manner similar to that described in the patent (20). Four grams of ammonium niobium oxalate dissolved in 18 ml hot

[1] Current address: Catalysis Research Center, Hokkaido University, Kita-ku, Sapporo 060-0811, Japan.

[2] Current address: Department of Material Science, Shimane University, 1060 Nishikawazu, Matsue 690-8504, Japan.

[3] To whom correspondence should be addressed: Fax: 81-3-5800-6892. E-mail: iwasawa@chem.s.u-tokyo.ac.jp.

0021-9517/00 $35.00

water was added to another 117 ml hot aqueous solution of 4.2 g ammonium metavanadate, 15.9 g ammonium para-polymolybdate, and 4.1 g orthotelluric acid. The resultant orange slurry was dried at 423–523 K to form dark green-brown powder. The sample was then treated at 873 K for 2 h under a flow of He or N_2 (11 ml/min). The catalyst was obtained as black powder.

The surface area of the sample was measured by the BET method (BELSORP 28SA). X-ray powder diffraction (XRD) was recorded on a Rigaku X-ray diffractometer (CN4026A1; 35 kV, 15 mA), where Cu $K\alpha$ radiation was used with a Ni filter. X-ray fluorescence (XRF) measurement was carried out on a Seiko SEA2010 XRF spectrometer with an Rh target operated at 50 kV with 1 mA . X-ray photoelectron spectra (XPS) were taken on Rigaku XPS-7000 (Mg $K\alpha$; 15 kV, 10 mA). The sample was pressed to a thin disk and attached to a Cu sample holder with double-sided conducting tape. Spectra were recorded for V $2p_{3/2}$, Mo $3d_{5/2}$, Nb $3d_{5/2}$, Te $3d_{5/2}$, and O 1*s* regions. The binding energies were referred to 285 eV for C 1*s*.

The kinetic measurements were carried out in a fixed-bed flow reactor. The diameter of the reactor was 6 mmϕ. The catalytic reactions were performed at atmospheric pressure with composition of $C_3H_8/NH_3/O_2/He = 6/7/17/70$ (total flow rate was 6 ml/min) in the temperature range 693–773 K. The typical amount of charged catalyst was 0.5 g (catalyst volume was about 1.5 ± 0.4 cm^3). The products were analyzed by gas chromatography using a Porapak Q column for CO_2, NH_3, H_2O, hydrocarbons, and nitriles and with a Molecular Sieve 5A column for O_2, N_2, and CO.

Conversion, selectivity, and yield are defined as follows:

Propane conversion (%) $= (1 - C_{C3H8}/C^0_{C3H8}) \times 100$.
NH_3 conversion (%) $= (1 - C_{NH3}/C^0_{NH3}) \times 100$.
O_2 conversion (%) $= (1 - C_{O2}/C^0_{O2}) \times 100$.
Selectivity (%) for product P (carbon base) $= \nu_P C_P/(C^0_{C3H8} - C_{C3H8}) \times 100$.
Yield of product P (%) = Selectivity (%) $\times$ Conversion (%)/100.
C_X: mole of the component X in the effluent gas.
C^0_X: mole of the component X in the feed gas.
ν^X: coefficient for the chemical reaction.

RESULTS

Catalyst Preparation and Catalytic Performance

In order to reproduce the high catalytic performance of the MoVNbTe oxide described in the patents (20–22), we examined the optimum preparation conditions for the active catalyst, changing the drying process, calcination temperature, and O_2 content during the calcination process. Good performance was obtained when an $MoV_{0.4}Nb_{0.1}Te_{0.2}$ oxide was pretreated in the temperature range 870–900 K for 2 h under 10 ml/min He or N_2 flow. The optimal MoVNbTe oxide catalyst showed a conversion of 87% with an acrylonitrile selectivity of 55% at 693 K and a conversion of 90% with an acrylonitrile selectivity of 46% at 723 K under flow conditions of $C_3H_8/NH_3/O_2/He = 6/7/17/70$% and 6ml/min ($W/F = 0.083$ g-cat $\cdot$ min $\cdot$ ml^{-1}) as shown in Table 1. These results reproduce the performance reported in the patents (20–22). The higher or lower calcination temperatures provided less active catalysts as compared to those prepared under the above conditions. Another key issue in obtaining high-performance catalysts was the O_2 contamination in a N_2 flow during the calcination process. Figure 1 shows the dependence of the performance of propane ammoxidation on the O_2 concentration. When

TABLE 1

Performance of the MoVNbTe Oxide Catalysts and Other Multicomponent Oxide Catalysts for Propane Ammoxidation

Catalyst	Propane conv. (%)	O_2 conv. (%)	Propene selec. (%)	ACN[a] selec. (%)	CO_x selec. (%)	Ref.
$MoV_{0.4}Nb_{0.1}Te_{0.2}O_x$[b]						this work
693 K	87	98	7.9	55	33	
723 K	90	99	1.7	46	48	
$MoV_{0.32}Nb_{0.13}Te_{0.2}O_n$[c]	92.7			57.5		(20)
VSbOx[d]	75		2	20	75	(8, 48)
	20		4	8	44	
AgBiVMoO[e]	15.8	50.2	7.8	64.9	15.3	(49)
$VSbWP/Al_2O_3$[f]	85			37		(50)

[a] ACN: acrylonitrile.
[b] $C_3H_8 : NH_3 : O_2 : He = 6 : 7 : 17 : 70$ (%), $W/F = 0.083$ g-cat $\cdot$ min $\cdot$ ml^{-1} (=720 ml g-cat$^{-1} \cdot$ h^{-1}).
[c] $C_3H_8 : NH_3$: Air = 1 : 1.2 : 15 (volume ratio), GHSV = 1000 h^{-1}, 693 K.
[d] $C_3H_8 : NH_3 : O_2 = 1.2 : 15.3 : 15.2$ (%), balanced with He, 6480 ml g-cat$^{-1} \cdot$ h^{-1}, 773 K.
[e] $C_3H_8 : NH_3 : O_2 = 44 : 15 : 41$ (%) 3000 ml g-cat$^{-1} \cdot$ h^{-1}, 788 K.
[f] $C_3H_8 : NH_3 : O_2 : H_2O = 1 : 2 : 3 : 6$ balanced with He, 773 K.

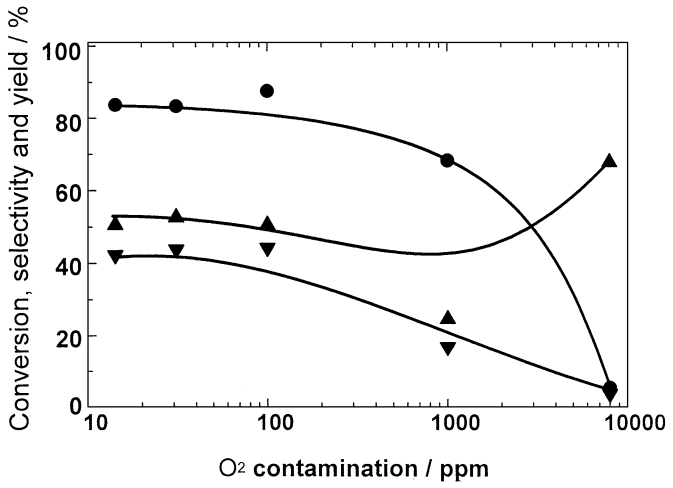

FIG. 1. Dependence of propane conversion (●), selectivity to acrylonitrile (ACN) (▲), and ACN yield (▼) on the O_2 contamination in an N_2 flow for the catalyst pretreatment. Pretreatment temperature: 900 K. The propane ammoxidation reactions were carried out under the same conditions as in Table 1.

the O_2 concentration exceeded 1000 ppm, the propane conversion dramatically decreased. The conversion became as low as 6% when the O_2 contamination in the N_2 flow was 8000 ppm.

Reaction Kinetics

Figure 2a shows the effect of space velocity on the conversions of propane and oxygen, and the yields of the various reaction products. The yields of propene and acrylonitrile passed through a maximum with increasing contact time (W/F), while the CO_x formation constantly increased with W/F. Figure 2b shows the relation between the propane conversion and the selectivities to the products. Note that the selectivities to acrylonitrile and propene did not change significantly as the conversion increased up to 90%, while at 95% conversion the selectivity of acrylonitrile dropped. This dependence of the selectivities to acrylonitrile and propene on the propane conversion is unique compared to the corresponding dependence reported for $VSbO_x$ (14).

The MoVNbTe oxide catalyst can convert propene to acrylonitrile with a high selectivity. Figures 3a and 3b show the effect of space velocity on the yield and conversion in the propene ammoxidation at 693 K, respectively. Since the activity (conversion) was much higher, we collected the data at higher flow rates. The gas composition was similar to that in the propane ammoxidation, i.e., propene: $NH_3 : O_2 : He = 6 : 7 : 17 : 70$ (%). Acrylonitrile was a major product in the wide range of W/F, typically 75% selectivity at 70% conversion.

The activation energies for the propane ammoxidation on the optimal MoVNbTe oxide catalyst between 663 and 723 K were calculated under low conversion con-

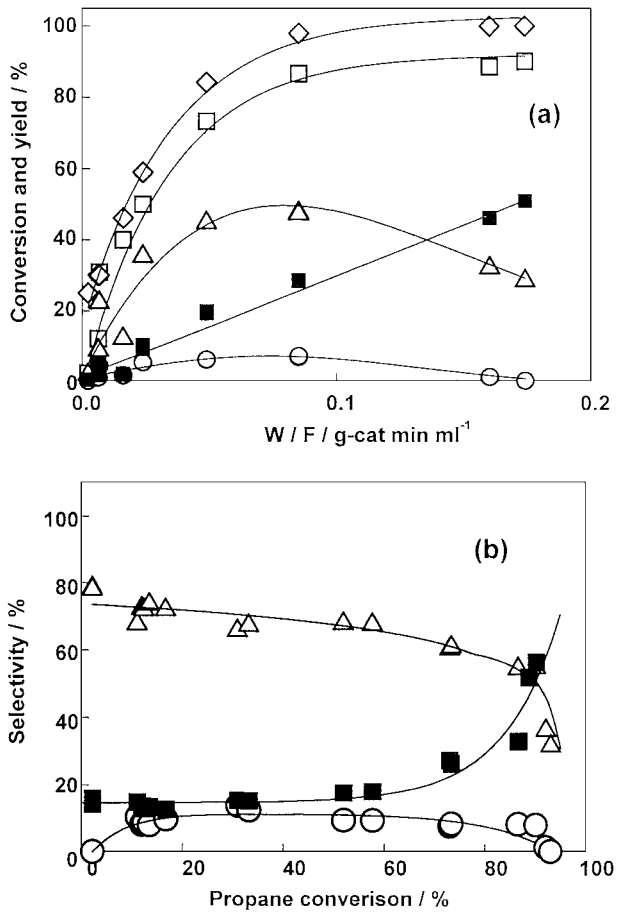

FIG. 2. (a) Conversions of propane (□) and O_2 (◇) and yields of ACN (△), C_3H_6 (○) and COx (■) as a function of W/F in the propane ammoxidation at 693 K and propane: $NH_3 : O_2 : He = 6 : 7 : 17 : 70$ (%) on the MoVNbTe oxide catalyst. (b) Selectivities to ACN (△), C_3H_6 (○), and CO_x (■) as a function of the C_3H_8 conversion.

ditions (around 10% propane conversion) by increasing flow rates (100 ml/min, $W/F = 0.005$ g-cat · min · ml^{-1}), and they are tabulated in Table 2, together with those for the propene ammoxidation. The activation energies for the propane conversion and the formation of acrylonitrile and propene were almost the same, 32 kcal/mol, 34 kcal/mol,

TABLE 2

Apparent Activation Energies (kcal mol^{-1}) for the Ammoxidation of Propane and Propene on $MoV_{0.4}Nb_{0.1}Te_{0.2}O_x$

	C_3 conv.	NH_3 conv.	O_2 conv.	CO prod.	CO_2 prod.	C_3H_6 prod.	ACN prod.
C_3H_8	32 ± 1	17 ± 1	19 ± 2	55 ± 1	15 ± 1	33 ± 1	34 ± 1
C_3H_6	36 ± 1	31 ± 1	29 ± 1	58 ± 1	25 ± 1		39 ± 1

Note. ACN: acrylonitrile. Temperature range: 663–723 K. Flow rate: 100 ml/min. Weight of catalyst: 0.5 g. Gas composition: $C_3H_8 : NH_3 : O_2 : He = 6 : 7 : 17 : 70$ (%).

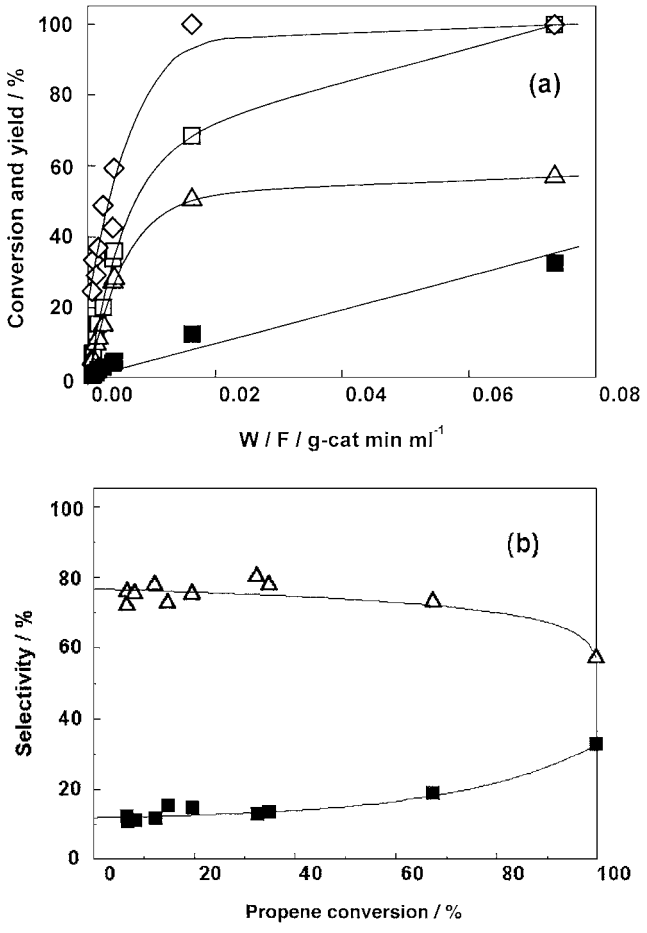

FIG. 3. (a) Conversions of propene (□) and O_2 (◇) and yields of ACN (△) and CO*x* (■) as a function of *W*/*F* in propene ammoxidation at 693 K for propene: NH_3 : O_2 : He of 6 : 7 : 1 : 70 (%) on the MoVNbTe oxide catalyst. (b) Selectivities to ACN (△) and CO_x (■) as a function of the C_3H_6 conversion.

and 33 kcal/mol, respectively. The CO_2 formation showed a much lower activation energy of 15 kcal/mol. In the propene ammoxidation the activation energies for the propene conversion and the formation of acrylonitrile were 36 and 39 kcal/mol, respectively, a little larger than those for propane ammoxidation though the catalytic activity for propene ammoxidation was larger than that for propane ammoxidation.

Figure 4 shows the reaction rates as a function of the reactant concentration. The reaction rates were evaluated under differential conditions. A standard gas composition of propane: NH_3 : O_2 was 6% : 7% : 17% balanced with He (70%). Concentration of this gas was varied, while those of the other gases were kept constant. The total flow rate was fixed at 100 ml/min by being balanced with He. The rates of propane conversion and acrylonitrile formation increased with increasing propane and O_2 concentrations. We could not find saturation values in the reaction rate under the reaction conditions. On the other hand, increasing NH_3 concentration suppressed C_3H_8 conversion and acrylonitrile formation. The reaction orders are listed in Table 3. The reaction orders with respect to propane, NH_3, and O_2 for acrylonitrile formation were 0.8, −0.5, and 0.4, respectively, and those for the total conversion were 0.8, −0.4, and 0.4, respectively.

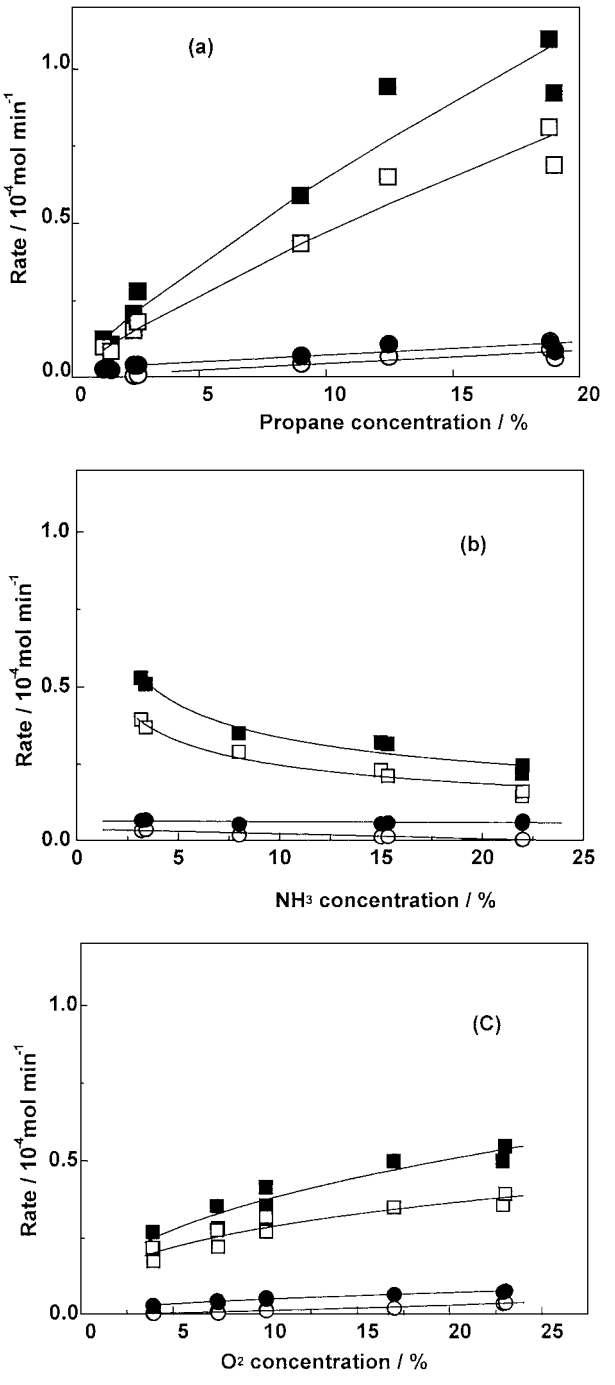

FIG. 4. Rates for propane conversion (■) and acrylonitrile (□), C_3H_6 (○), and CO_x (●) formation at 693 K on the MoVNbTe oxide catalyst as a function of the concentrations of propane (a), NH_3 (b), and O_2 (c); $W/F = 0.0005$ g-cat min ml^{-1}. C_3H_8 : NH_3 : O_2 : He = 6 : 7 : 17 : 70.

TABLE 3

Apparent Reaction Orders for Propane Ammoxidation on $MoV_{0.4}Nb_{0.1}Te_{0.2}O_x$

	C_3 conv.	NH_3 conv.	O_2 conv.	CO prod.	CO_2 prod.	C_3H_6 prod.	ACN prod.
$\gamma 1$	0.8 ± 0.2	0.0 ± 0.1	0.1 ± 0.1	0.9 ± 0.2	0.5 ± 0.2	1.3 ± 0.2	0.8 ± 0.2
$\gamma 2$	-0.4 ± 0.1	0.5 ± 0.2	0.4 ± 0.1	-1.0 ± 0.1	0.0 ± 0.1	-0.7 ± 0.3	-0.5 ± 0.2
$\gamma 3$	0.4 ± 0.2	0.2 ± 0.1	0.2 ± 0.1	0.5 ± 0.2	0.6 ± 0.1	1.4 ± 0.3	0.4 ± 0.2

Note. $V = [C_3H_8]^{\gamma 1}[NH_3]^{\gamma 2}[O_2]^{\gamma 3}$. Temperature: 693 K. Flow rate: 100 ml/min. Weight of catalyst: 0.5 g. Standard feed gas composition: $C_3H_8 : NH_3 : O_2 : He = 6 : 7 : 17 : 70$ (%).

BET, XRD, and XPS Analyses

The optimal $MoV_{0.4}Nb_{0.1}Te_{0.2}$ oxide catalyst showed a BET surface area of 2.5 ± 0.5 m^2/g. Calcination under the more O_2-contaminated He flow reduced the surface area. When the sample was calcined under an He flow with 1000 ppm or 8000 ppm O_2 contamination, the surface areas of these samples were 1.8 and 0.5 m^2/g, respectively. Accordingly, the activity of propane ammoxidation reaction decreased on these catalysts.

Figure 5 depicts XRD patterns for the samples calcined with He flow of different O_2 concentrations. The sample with the highest activity gave XRD peaks at $2\theta = 22.1°$, 28.2°, 36.2°, 44.7°, and 50.0°, which corresponded to the peaks reported in the patents as active species (20, 22). In addition, there were many other peaks. Especially in the active catalysts; the remarkable peaks appeared at 7.7°, 9.0°, 14.1°, 24.9°, 26.5°, 26.9°, 29.1°, 31.1°, 32.4°, 33.2°, and 35.4°. As the O_2 contamination in the He flow increased, the intensity of the peaks reported in the patent decreased and new peaks corresponding to α-MoO_3 appeared at 12.6°, 23.3°, 25.6°, 27.2°, and 38.9°. The peaks at 7.7° and 9.0° also increased, but the peaks at 14.1°, 22.1°, 24.9°, 28.2°, 32.4°, and 33.2° decreased. Variation of other remarkable peaks appearing in the active catalyst was unclear due to overlapping of XRD peaks in the range 22°–40°. No peaks corresponding to V_2O_5 or Nb_2O_5 were observed in the XRD patterns even under the highly O_2-contaminated conditions.

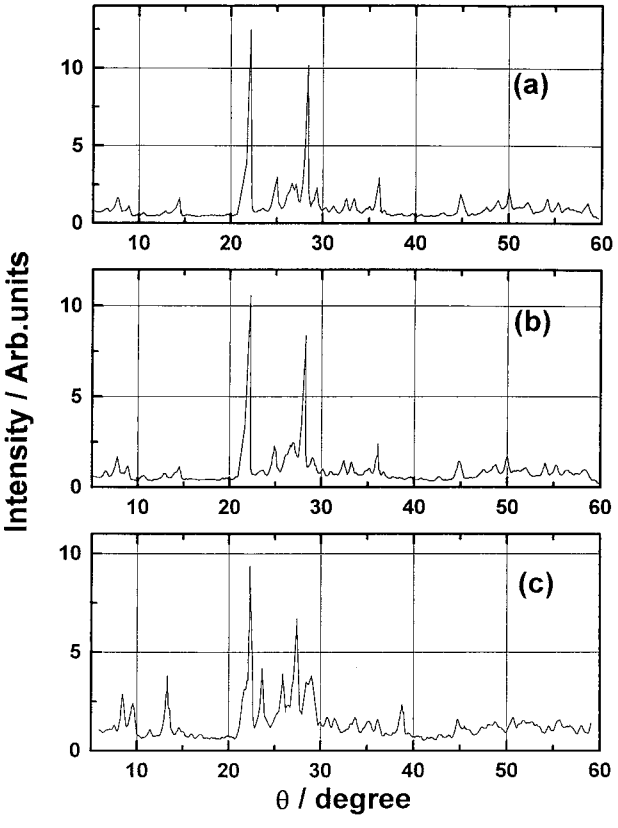

FIG. 5. XRD patterns for the MoVNbTe oxide catalysts calcined in an He flow with different O_2 contamination; (a) 20, (b) 1000, (c) 8000 ppm.

Figure 6 shows the XPS at V $2p_{3/2}$, Mo $3d_{5/2}$, Nb $3d_{5/2}$, and Te $3d_{5/2}$ regions for the catalyst pretreated under different O_2-concentration He flows at 873 K. The binding energies and the peak widths are given in Table 4. As the O_2 content in the He gas increased, the peak width of Mo $3d_{5/2}$ gradually decreased, while the binding energy remained unchanged, corresponding well to that of Mo^{6+}. This may be partly due to a decrease in the amount of Mo^{5+} species which may be formed during the O_2-free or lower-O_2-content calcination processes. The Mo $3d_{5/2}$ and $3d_{3/2}$ peaks of the sample treated with the low-O_2-content (20 ppm) He flow are deconvoluted in Fig. 7a, which shows peaks at 232.7 and 232.0 eV for Mo $3d_{5/2}$ with a peak ratio of 2 : 1. The former peak is straightforwardly assigned to Mo^{6+} because the binding energy of MoO_3 is about 232.5 eV. Swartz and Hercules reported the correlation between XPS binding energy (E_{bind}) and Mo valence (Z) for

TABLE 4

Binding Energies (Peak Widths) of Mo, V, Nb, and Te XPS for the $MoVNbTeO_x$ Catalysts Prepared under Different O_2 Concentration in the He Flow

O_2 content (ppm)	Mo $3d_{5/2}$ (eV)	V $2p_{3/2}$ (eV)	Nb $3d_{5/2}$ (eV)	Te $3d_{5/2}$ (eV)
20	232.5(1.9)	516.7(1.6)	206.3(1.5)	576.2(2.0)
100	232.6(1.8)	516.6(1.6)	206.6(1.6)	576.3(1.9)
1000	232.6(1.7)	516.5(1.6)	206.6(1.6)	576.3(2.1)
8000	232.8(1.6)	516.5(1.6)	206.3(1.6)	576.2(2.0)

Note. The energy was referred to 285 eV of C 1*s*.

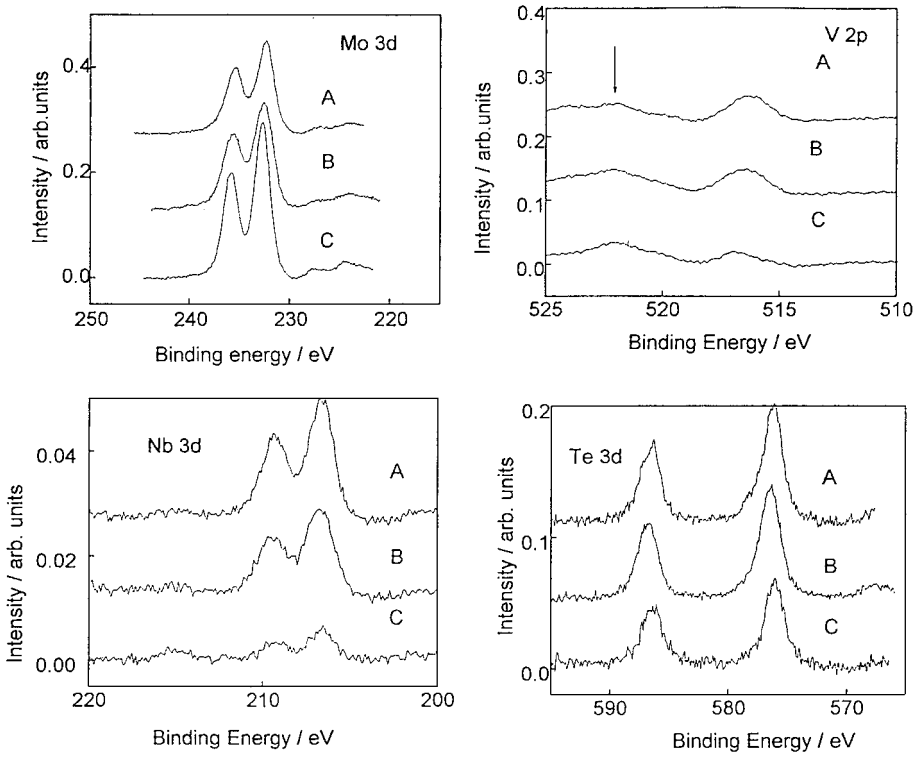

FIG. 6. XPS spectra in the Mo 3*d*, V 2*p*, Nb 3*d*, and Te 3*d* binding energy region for the MoVNbTeOx catalysts calcined under an He flow with O_2 content of (A) 20 (B) 1000, and (C) 9000 ppm. The arrow in the V 2*p* spectra indicates an O Mg $K\alpha_{3,4}$ satellite peak.

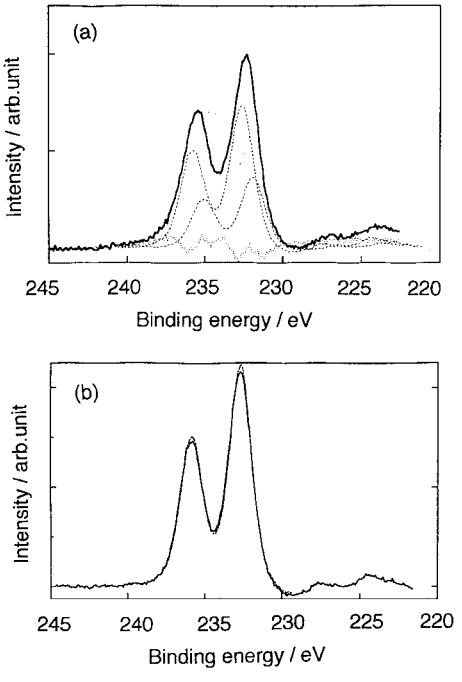

FIG. 7. Deconvolution of the Mo $3d_{5/2}$ and $3d_{3/2}$ peaks for the MoVNbTeOx oxide catalysts calcined under the 20 ppm O_2 contaminated He flow (a) and the 9000 ppm O_2 contaminated He flow (b). Solid line: observed data. Broken lines: deconvoluted peaks. Dotted line: residual.

Mo oxides; $E_{\text{bind}} = 0.972Z + 226.5$ (2b). Thus the peak observed at 232.0 eV can be ascribed to Mo^{5+}. We did not observe any peak at lower binding energies. It is also indicated that the Mo species after pretreatment under the lower-O_2-concentration flow conditions is composed of Mo^{6+} and Mo^{5+} species. On the other hand, Fig. 7b depicts the deconvolution of the Mo $3d_{5/2}$ and $3d_{3/2}$ peaks for the catalyst prepared under 9000 ppm O_2-contaminated conditions, where the peaks were fitted with a single component of Mo^{6+}.

The binding energies of V $2p_{3/2}$ and Nb $3d_{5/2}$ were 516.7 and 206.7 eV, respectively. The V $2p_{1/2}$ peak was completely hindered by a peak appearing at 522 eV which is due to Mg $K\alpha_{3,4}$ satellites of O 1*s*. Hence the width of the V $2p_{3/2}$ peak might be less reliable owing to the presence of the satellite peak. However, we could estimate the peak position of V $2p_{3/2}$ because the energy separation of V $2p_{3/2}$ and the satellite peak was as large as 5 eV. The V $2p_{3/2}$ binding energies of reference compounds, V_2O_5 and VO_2 are 517.0 and 516.0 eV, respectively. Therefore the V valence state in the catalyst may be 5+ or a little reduced. The Nb $3d_{5/2}$ binding energies for Nb_2O_5 and NbO_2 were 207.0 and 205.5 eV, respectively. Thus Nb is also in a 5+, or a little less, oxidation state. The Te 3*d* peak appeared at 576.2 eV, corresponding to Te^{4+}. The Te ions in the catalyst were reduced from Te^{6+} to Te^{4+} during the calcination process. We never found Te^0 on the catalyst surface. The binding energies of V $2p_{3/2}$,

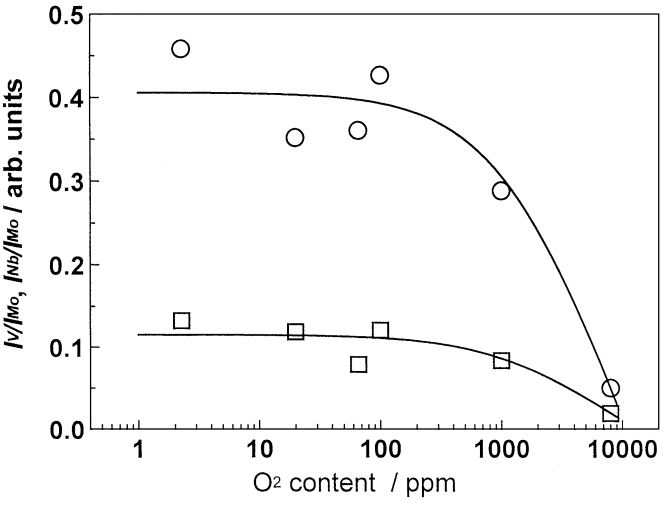

FIG. 8. XPS intensity ratios of V $2p_{3/2}$ (○) and Nb $3d_{5/2}$ (□) to Mo $3d_{5/2}$ as a function of O_2 content in the calcination gas.

Nb $3d_{5/2}$, and Te $3d_{5/2}$ for the 8000 ppm O_2 calcined sample were 516.5, 206.7, and 576.2 eV, respectively. The shifts of the binding energies from those for the 20 ppm O_2 calcined sample were less than 0.3 eV, which indicates that the valence states of these elements are almost the same in both catalysts. However, the peak intensities of V and Nb greatly diminished after the 8000 ppm O_2 calcination.

Figure 8 shows the XPS intensity ratio of V $2p_{3/2}$, and Nb $3d_{5/2}$ to Mo $3d_{5/2}$. The intensity of the V peak in the MoVNbTe oxide catalyst treated in the 8000 ppm O_2-contaminated gas was as small as 1/5 of that in the catalyst obtained in the 20 ppm O_2-contaminated gas. The intensity of the Nb peak also decreased with the O_2 content in the calcination gas. The atomic ratio in the bulk determined by XRF analysis was Mo : V : Nb = 1 : 0.37 : 0.09 after the treatment with an O_2 content of 20 ppm. The value did not significantly change after the treatment under the 8000 ppm O_2 content He flow. Thus the decrease in the XPS peak intensity is not due to the change in the bulk concentration but is due to the decrease in the surface concentration of V and Nb. Comparing the XPS data with the activity data in Fig. 1, the decrease in the activity can be correlated with the decrease in the concentration of V and Nb at the catalyst surface. The structural origin for the decrease in the activity of the MoVNbTe oxide catalyst under the O_2-rich conditions is relevant to the following four factors: (1) decrease in the surface area, (2) decrease in the active phase and formation of α-MoO_3, (3) decrease in the Mo^{5+} species, and (4) decrease in the surface V and Nb content.

DISCUSSION

XRD and Active Phase

Ushikubo *et al.* first reported active species for propane ammoxidation which gave XRD peaks at $2\theta = 22.1°$, 28.2°, 36.2°, 44.7°, and 50.0° (20, 22). Recently they reported another new phase possessing XRD peaks at $2\theta = 9.0°$, 22.1°, 27.3°, 29.2°, and 35.4° (24). They called the latter phase active phase M1 and the former M2. It has been proposed that phase M1 is relevant to activation of propane to form propene as intermediate and phase M2 converts the propene selectively to acrylonitrile through allyl intermediate transfer (24). In the present paper we found distinct peaks at $2\theta = 7.7°$, 9.0°, 14.1°, 22.1°, 24.9°, 26.5°, 26.9°, 28.2°, 29.1°, 31.1°, 32.4°, 33.2°, 35.4°, 36.2°, 44.7°, and 50.0° for the active MoVNbTe catalyst. The peaks at 7.7°, 14.1°, 24.9°, 26.5°, 31.1°, 32.4°, and 33.2° are newly observed ones in this work. The peak at 26.9° may correspond to the one at 27.3° reported in the literature (24). Compared with the peaks in the less active catalyst prepared in the more O_2-contaminated calcination gas, the XRD peaks at 14.1° (new), 22.1° (M2), 24.9° (new), 28.2° (M2), 29.1° (M1), 32.4° (new), 33.2° (new), 35.4° (M1), 36.2° (M2), 44.7° (M2), and 50.0° (M2) seem to be relevant to the high conversion of propane to acrylonitrile. We tentatively denote this phase "active phase X." The peaks at 7.7° and 9° retained or increased their intensity even in the low activity catalysts. The peaks at 7.7° and 9° can be attributed to $(Nb_{0.09}Mo_{0.91})O_{2.8}$ ($a = 22.87$ Å, $c = 4.02$ Å, tetragonal) and $(V_{0.07}Mo_{0.93})O_{2.8}$ ($a = 22.84$ Å, $c = 3.99$ Å, tetragonal), which can give other peaks at 22.3°, 25.0°, 31.6°, and 33.2°. The 22.3°, 25.0°, and 33.2° peaks may overlap the peaks for "active phase X" or other unidentified phases. Ushikubo *et al.* attributed the 9° peak to the one for the active phase M1. These phases ($(Nb_{0.09}Mo_{0.91})O_{2.8}$ and $(V_{0.07}Mo_{0.93})O_{2.8}$) seem to not be directly related to the high performance because the 8000 ppm O_2 treated sample (less active catalyst) gave stronger 7.7° and 9° peaks than the other more active catalysts.

The high performance of the MoVNbTe oxide catalyst might arise from a combination of MoVNb oxide and MoTe oxide. $Mo_xV_yNb_zO_w$ shows a high activity for oxidative dehydrogenation of ethane to ethene when $x = 0.7$–0.8, $y = 0.1$–0.2, and $z = 0.04$–0.1 (27–31). Many XRD peaks were observed in the range $2\theta = 22°$–$30°$. These peaks are attributed to a multiphase of MoO_3, $Mo_6V_9O_{40}$, $Mo_4V_6O_{25}$, and $Mo_3Nb_2O_{11}$. $Mo_6V_9O_{40}$ and $Mo_4V_6O_{25}$ should give a strong peak at $\theta = 21.6°$ ($d = 4.06$ Å), which we could not find in the active MoVNbTe oxide catalyst. Thorsteinson *et al.* correlated the activity of the MoVNb oxide catalyst with the intensity of an XRD peak at $2\theta = 22.2°$ ($d = 4.0$ Å) (27). Burch *et al.* attributed the peak at $2\theta = 22.2°$ to $Mo_3Nb_2O_{11}$ (28). The $Mo_3Nb_2O_{11}$ gave a strong peak at 27.6°, which we could not find in the MoVNbTe oxide catalyst either. Thus the crystal structure found in MoVNbTe oxide was different from those found in the MoVNb oxide catalyst. Ruth *et al.* claimed that the active phase of the MoVNb oxide catalyst was not due to the crystalline phase but to the amorphous phase with a composition of $Mo_{0.84}V_{0.13}Nb_{0.02}O_x$ and that Nb played a role in

stabilizing this amorphous phase (30). They also stated that low-temperature calcination (673 K) was essential to preserve the active amorphous phase. In the MoVNbTe oxide catalyst, the activity appears after the high-temperature treatment at 773 K and good crystalline phases are always found. Thus the active phases should be present in a crystalline state. Moreover the crystalline state should include Te atoms because in the MoVNb oxide system Mo^{6+} was easily reduced to form Mo^{4+} under the reductive calcination conditions adopted in the present work (31), whereas the Mo in the MoVNbTe oxide system was found to be in 5+ and 6+.

Te has been used as an additive to increase the selectivity of acrylic acid synthesis from propene (7, 32–35). The addition of TeO_2 to V_2O_5–P_2O_5 enhances the propene oxidation activity for the formation of acrylic acid and acrolein (35). Selective oxidation of propene to acrylic acid proceeds on an NiMoTeO catalyst in the presence of water (32–34). It was suggested that the oxidation of propene to acrolein took place on Te-rich sites and that the further oxidation of acrolein to acrylic acid proceeded on the Te-poor sites. Thus Te seems to be a key component for selective oxidation reactions. MoTe oxides are also active for the selective oxidation and ammoxidation of propene (36). The active phase was suggested to be $MoTe_2O_7$, in which the propene activation occurred at the Te site and oxygen incorporation occurred at the Mo site. In the MoVNbTe oxide catalyst, the $MoTe_2O_7$ phase was not observed, which should have had strong peaks at $2\theta = 23.5^\circ$ and 26.7°. $MoTe_5O_{16}$, which shows $2\theta = 21.8^\circ$ and 26.6°, has been reported to be produced under reductive conditions. It was not observed either. Thus the "active phase X" in the MoVNbTe oxide catalyst is not a simple combination of the reported MoVNb and MoTe oxides. It may be composed of new phases containing all four metal elements in a crystalline state. In this work we could not get direct information about the number of active phases. Indexing of the diffraction peaks has been unsuccessful as yet, but the complicated separations of the lattice plane (*d*-values) indicate that "active phase X" is composed of two or more phases. Further study is necessary to characterize the multioxide phases and to find the correlation between the ammoxidation activity and each crystalline oxide phase.

Oxidation States in Active Phases

The Mo $3d_{5/2}$ peak became a little sharper (Table 4) and the intensities of the V $2p_{3/2}$ and Nb $3d_{3/2}$ peaks decreased with the increase of O_2 concentration (Fig. 8). The peak deconvolution analysis for Mo $3d_{5/2}$ in the active MoVNbTe oxide catalyst prepared under the 20 ppm O_2 contaminated flow condition revealed the presence of Mo^{5+} (Fig. 7). After the treatment of the catalyst in the 8000 ppm O_2 containing He flow, α-MoO_3 phase was mainly formed at the surface layers with little Mo^{5+}. This surface change was responsible for the degradation of the activity (Fig. 1). We think that Mo^{5+} is involved in active phase X, as discussed above. Thornsteinson *et al.* also stated that the MoNbV oxide catalysis for the ethane dehydrogenation was relevant to the presence of Mo^{5+} (27). The V $2p_{3/2}$ peak in the MoVNbTe oxide catalyst was observed at 516.7 eV, which is lower by 0.3 eV than that for V_2O_5. There may exist V^{4+} ions in addition to the majority of V^{5+} ions. A similar amount of shift to a lower binding energy was also reported for the V $2p_{3/2}$ binding energy of a VSbOx catalyst (37, 38). V is a key component in many oxidation reactions of alkanes (7), but V^{5+}oxides are also active for the total oxidation of alkanes and the undesired decomposition of NH_3 to N_2 (2, 37). The partially reduced V^{4+} states stabilized in the multicomponent oxide may contribute partly to the high performance for propane ammoxidaiton.

Nb_2O_5 is not active but is selective for the dehydrogenation reaction of propane to propene (39, 40). Desponds *et al.* reported that the addition of Nb to an MoV oxide catalyst increased the selectivity to ethene in the oxidative dehydrogenation of ethane (29). Smits *et al.* demonstrated that the addition of V or Cr to Nb oxide increased the propane dehydrogenation activity (41, 42). Matsuura *et al.* suggested that the combination of V and Nb increased the acidity of the sample (43). Thus Nb may also play an important role in "active phase X," enhancing the acidity and selectivity.

The features of the multicomponent MoVNbTe oxide catalyst are characterized by: (i) isolation of active V and Mo sites, (ii) stabilization of low valence states (Mo, V), (iii) prevention of overreduction (Mo), (iv) enhancement of acidity (Nb), and (v) formation of active ensembles ($MoVNbTeO_y$).

Reaction Kinetics and Mechanism

Here we summarize the kinetic parameters and activation energies and discuss a possible reaction mechanism. The activation energies for propane and propene ammoxidation on the MoVNbTe oxide catalyst were 32 and 36 kcal/mol, respectively. It is to be noted that the activation energy for propene ammoxidation is a little larger than that for propane ammoxidation. The rate equations (reaction orders for C_3H_8, NH_3, and O_2 pressures) for both ammoxidations are also different, as shown in Table 3. These results suggest that the rate-determining step in propane ammoxidation may not be the dehydrogenation of propane to propene but a succeeding step during acrylonitrile synthesis or that propane is directly converted to an intermediate without passing through propene. Further, the difference in activation energy may be due to the different concentrations of adsorbed species such as NH_x under propane and propene ammoxidation conditions. Anyhow, it can be said that the MoVNbTe oxide is an excellent catalyst because it has high ability for C–H activation of saturated hydrocarbons like propane.

In the low conversion limit, the acrylonitrile selectivity increased to 80% and the CO_2 and CO selectivity decreased to 15%, while the C_3H_6 selectivity decreased to nearly zero. Centi *et al.* suggested the presence of two routes for the selective oxidation of propane on an $SbVO_x$ catalyst. One route involves propene as intermediate (major) and the other route proceeds via propionate intermediate (minor) (4, 15, 44–48). They also claimed that in the presence of ammonia the latter route was inhibited because of the NH_3 adsorption on Lewis acid sites. Catani *et al.* reported that the acrylonitrile formation on a $SbVO_x$ catalyst passed through a maximum as the propane conversion decreased, while the propene formation increased with decreasing propane conversion (15). However, in the MoVNbTe oxide catalyst, the propene formation passed through a maximum and the acrylonitrile formation increased with the decrease in the propane conversion, as shown in Fig. 2b. Thus the reaction features seem to be different from those for $SbVO_x$. More detailed spectroscopic study is necessary to discuss the reaction mechanism for propane ammoxidation on the MoVNbTe oxide catalyst.

ACKNOWLEDGMENTS

This work has been supported by the Core Research for Evolutional Science and Technology (CREST) project of the Japan Science and Technology Corporation (JST). We thank the High Intensity X-Ray Facility of the Graduate School of Engineering, The University of Tokyo, for measurements of XPS spectra.

REFERENCES

1. Grasselli, R. K., *Catal. Today* **49**, 141 (1999).
2. Moro-oka, Y., and Ueda, W., *Adv. Catal.* **40**, 233 (1994).
3. Grasselli, R. K., *in* "Handbook of Heterogeneous Catalysis" (G. Ertl, H. Knözinger, and J. Weitkamp, Eds.), Chap. 4.6.6, p. 2302. Wiley–VCH, New York, 1997.
4. Centi, G., Perathoner, S., and Trifiro, F., *Appl. Catal. A* **157**, 143 (1997).
5. Mamedov, E. A., and Corberan, V. C., *Appl. Catal.* **127**, 1 (1995).
6. Sokolovskii, V. D., Davydov, A. A., and Ovsitser, O. Y., *Catal. Rev.* **37**, 425 (1995).
7. Albonetti, S., Cavani, F., and Trifiro, F., *Catal. Rev.* **28**, 413 (1996).
8. Bettahar, M. M., Costentin, G., Savary, L., and Lavalley, J. C., *Appl. Catal. A* **145**, 1 (1996).
9. Centi, G., and Peerathoner, S., *Catal. Rev.* **40**, 175 (1998).
10. Kim, Y. C., Ueda, W., and Moro-Oka, Y., *Catal. Today* **13**, 673 (1992).
11. Guttman, A. T., Grasselli, R. K., Brazdil, J. F., and Suresh, D. D., U.S. Patent 4788317 (1988).
12. Guttman, A. T., Grasselli, R. K., Brazdil, J. F., and Suresh, D. D., U.S. Patent 4797381 (1988).
13. Grasselli, R. K., Centi, G., and Trifiro, F., *Appl. Catal.* **57**, 149 (1990).
14. Andersson, A., Andersson, S. L. T., Centi, G., Grasselli, R. K., Sanati, M., and Trifiro, F., "Proceedings 10th International Congress on Catalysis, Budapest, 1992" (L. Guczi, F. Solymosi, and P. Tetenyi, Eds.), p. 691. Akadémiai Kiadó, Budapest, 1993.
15. Catani, R., Centi, G., Trifiro, F., and Grasselli, R. K., *I&EC Res.* **31**, 107 (1992).
16. Inoue, T., Asakura, K., and Iwasawa, Y., *J. Catal.* **171**, 184–190 (1997).
17. Inoue, T., Asakura, K., and Iwasawa, Y., *J. Catal.* **171**, 457 (1997).
18. Inoue, T., Asakura, K., Li, W., Oyama, S. T., and Iwasawa, Y., *Appl. Catal. A Gen.* **165**, 183 (1997).
19. Iwasawa, Y., Asakura, K., and Inoue, T., U.S. Patent 5864051 (1997).
20. Ushikubo, T., Kayou, A., Oshima, K., and Umezawa, T., JP 5-208136 (1993).
21. Ushikubo, T., Nakamura, H., Koyasu, Y., and Wajiki, S., EP 0608838A2 (1994).
22. Ushikubo, T., Sawaki, I., Oshima, I., Kiyono, K., and Inumaru, K., JP 7-232071 (1995).
23. Vaarkamp, M., and Ushikubo, T., *Appl. Catal.* **174**, 99 (1998).
24. Ushikubo, T., Oshima, K., Kayou, A., and Hatano, M., *in* "Spillover and Migration of Surface Species on Catalysts" (C. Li and Q. Xin, Eds.), Stud. Surf. Sci. Catal., Vol. 112, p. 473, 1997.
25. Ushikubo, T., Oshima, K., Kayou, A., Vaarkamp, M., and Hatano, M., *J. Catal.* **169**, 394 (1997).
26. Swartz, J. W. E., and Hercules, D. M., *Anal. Chem.* **43**, 1774 (1971).
27. Thorsteinson, E. M., Wilson, T. P., Young, F. G., and Kasai, P. H., *J. Catal.* **52**, 116 (1978).
28. Burch, R., and Swarnakar, R., *Appl. Catal.* **70**, 129 (1991).
29. Desponds, O., Keiski, R. L., and Somorjai, G. A., *Catal. Lett.* **19**, 17 (1993).
30. Ruth, K., Burch, R., and Kieffer, R., *J. Catal.* **175**, 27 (1998).
31. Ruth, K., Kieffer, R., and Burch, R., *J. Catal.* **175**, 16 (1998).
32. Bart, J. C. J., Bossi, A., Petrini, G., Battiston, G., Castellan, A., and Covini, R., *Appl. Catal.* **4**, 153 (1982).
33. Jaeger, P., and Germain, J. E., *Bull. Soc. Chim. Fr.* **1**, 407 (1982).
34. Bart, J. C. J., Bossi, A., Petrini, G., Battiston, G., Castellan, A., and Covini, R., *Appl. Catal.* **6**, 85 (1984).
35. Ai, M., *J. Catal.* **101**, 473 (1986).
36. Bart, J. C. J., and Giordano, N., *J. Catal.* **64**, 356 (1980).
37. Andersson, A., Andersson, S. L. T., Centi, G., Grasselli, R. K., Sanati, M., and Trifiro, F., *Appl. Catal.* **113**, 43 (1994).
38. Nilsson, R., Lindblad, T., and Andersson, A., *J. Catal.* **148**, 501 (1994).
39. Smits, R. H. H., Seshan, K., and Ross, J. R. H., *J. Chem. Soc. Chem. Commun.*, 558 (1988).
40. Smits, R. H. H., Seshan, K., and Ross, J. R. H., *in* "New Developments in Selective Oxidation by Heterogeneous Catalysts" (P. Ruiz and B. Delmon, Eds.), Stud. Surf. Sci. Catal., Vol. 72, p. 221. Elsevier, Amsterdam, 1992.
41. Smits, R. H. H., Seshan, K., Leemreize, H., and Ross, J. R. H., *Catal. Today* **16**, 513 (1993).
42. Smits, R. H. H., Ph.D. thesis, University of Twente, The Netherlands, 1994.
43. Matsuura, I., T., I., Hayakawa, S., and Kimura, N., *Catal. Today* **28**, 133 (1998).
44. Nilsson, R., Lindblad, T., and Andersson, A., *J. Catal.* **148**, 501 (1994).
45. Centi, G., and Parathoner, S., *Appl. Catal. A* **124**, 317 (1995).
46. Centi, G., Marchi, F., and Perathoner, S., *J. Chem. Soc. Faraday Trans.* **92**, 5141 (1996).
47. Centi, G., Marchi, F., and Perathoner, S., *J. Chem. Soc. Faraday Trans.* **92**, 5151 (1996).
48. Centi, G., Marchi, F., and Perathoner, S., *Appl. Catal.* **149**, 225 (1997).
49. Kim, Y. C., Ueda, W., and Moro-Oka, Y., *Appl. Catal.* **70**, 175 (1991).
50. Centi, G., Pesheva, D., and Trifiro, F., *Appl. Catal.* **33**, 343 (1987).